SCIENCE CHINA
Earth Sciences

•RESEARCH PAPER•

March 2023 Vol.66 No.3: 528–546
https://doi.org/10.1007/s11430-022-1055-5

Projection of China's future runoff based on the CMIP6 mid-high warming scenarios

Jiayue ZHOU[1], Hui LU[1*], Kun YANG[1,2], Ruijie JIANG[1], Yuan YANG[3], Wei WANG[4] & Xuejun ZHANG[5,6]

[1] *Department of Earth System Science, Ministry of Education Key Laboratory of Earth System Modeling, Institute for Global Change Studies, Tsinghua University, Beijing 100084, China;*
[2] *National Tibetan Plateau Data Center, State Key Laboratory of Tibetan Plateau Earth System and Resource Environment, Institute of Tibetan Plateau Research, Chinese Academy of Sciences, Beijing 100101, China;*
[3] *Center for Western Weather and Water Extremes, Scripps Institution of Oceanography, University of California San Diego, San Diego 92037, USA;*
[4] *Changjiang Institute of Survey, Planning, Design and Research, Wuhan 430010, China;*
[5] *State Key Laboratory of Simulation and Regulation of Water Cycle in River Basin, China Institute of Water Resources and Hydropower Research, Beijing 100038, China;*
[6] *Research Center on Flood and Drought Disaster Reduction of the Ministry of Water Resources, Beijing 100038, China*

Received March 7, 2022; revised December 4, 2022; accepted December 26, 2022; published online February 13, 2023

Abstract The latest Coupled Model Intercomparison Project Phase 6 (CMIP6) proposes new shared pathways (SSPs) that incorporate socioeconomic development with more comprehensive and scientific experimental designs; however, few studies have been performed on the projection of future multibasin hydrological changes in China based on CMIP6 models. In this paper, we use the Equidistant Cumulative Distribution Function method (EDCDFm) to perform downscaling and bias correction in daily precipitation, daily maximum temperature, and daily minimum temperature for six CMIP6 models based on the historical gridded data from the high-resolution China Meteorological Forcing Dataset (CMFD). We use the bias-corrected precipitation, temperature, and daily mean wind speed to drive the variable infiltration capacity (VIC) hydrological model, and study the changes in multiyear average annual precipitation, annual evapotranspiration and total annual runoff depth relative to the historical baseline period (1985–2014) for the Chinese mainland, basins and grid scales in the 21st century future under the SSP2-4.5 and SSP5-8.5 scenarios. The study shows that the VIC model accurately simulates runoff in major Chinese basins; the model data accuracy improves substantially after downscaling bias correction; and the future multimodel-mean multiyear average annual precipitation, annual evapotranspiration, and total annual runoff depth for the Chinese mainland and each basin increase relative to the historical period in near future (2020–2049) and far future (2070–2099) under the SSP2-4.5 and SSP5-8.5 scenarios. The new CMIP6-based results of this paper can provide a strong reference for extreme event prevention, water resource utilization and management in China in the 21st century.

Keywords CMIP6, VIC model, EDCDFm, Chinese basins, Future hydrological changes

Citation: Zhou J, Lu H, Yang K, Jiang R, Yang Y, Wang W, Zhang X. 2023. Projection of China's future runoff based on the CMIP6 mid-high warming scenarios. Science China Earth Sciences, 66(3): 528–546, https://doi.org/10.1007/s11430-022-1055-5

* Corresponding author (email: luhui@tsinghua.edu.cn)

1. Introduction

The Sixth Assessment Report of the Intergovernmental Panel on Climate Change (IPCC AR6) indicates that the Earth's mean temperature has increased by 1.1°C relative to the preindustrial revolution period of 1850–1900 and that the rate of increase in global surface temperature in the period of 1970–2020 is greater than that in any 50-year period prior to 2000. Large amounts of greenhouse gases emitted by human activities are a primary cause of global warming (IPCC, 2021); furthermore, elevated CO_2 concentrations cause plant stomata to close, leading to reduced transpiration and thus affecting river flows (Gedney et al., 2006). Studies have shown (Skliris et al., 2016) that a 1°C increase will affect the hydrological cycle, amplifying the ambient humidity at a rate of 3–4%. Increasing temperature changes the total and seasonal peak of streamflow, which is mainly from snowmelt (IPCC, 2021) and in combination with abnormal weather, leads to hazards such as ice-rock collapse (Zhou et al., 2021). Global climate models (GCMs) can describe in detail the changes in atmospheric motion, heat exchange, and sea-land-air-ice interactions over time (Gleick, 1989) and are effective tools for studying the effects of historical, present, and future atmospheric changes on surface physical processes (Gonzalez et al., 2010; Sun et al., 2013; Guo et al., 2015). Coupled Model Intercomparison Project Phase 6 (CMIP6) has improved the simulation of temperature and precipitation in the China region compared with Coupled Model Intercomparison Project Phase 5 (CMIP5) (Jiang et al., 2020); specifically, the dry bias is significantly reduced in southern China (Zhu et al., 2020). CMIP6 is based on the Representative Concentration Pathways (RCPs) of CMIP5 (van Vuuren et al., 2011) and proposes the Shared Socioeconomic Pathways (SSPs) (Riahi et al., 2017), which can reflect newer and more diverse greenhouse gas concentration changes under social development (O'Neill et al., 2016). However, the spatial resolution of GCMs is coarse, and downscaling bias correction is usually required for finer-resolution basin-scale hydrological model simulations, where statistical downscaling is more widely used than dynamical downscaling due to simpler calculations and more reliable results (Ahmed et al., 2013).

Many studies have been done regarding the impact of future climate change on hydrology in China. At the single basin scale, Zhao et al. (2020) used 10 CMIP5 GCMs after statistical downscaling from the NEX-GDDP dataset (Sheffield et al., 2006) and two hydrological models, including variable infiltration capacity (VIC) (Liang et al., 1994), the study showed that runoff in the Xijiang River Basin increase in all seasons under the RCP4.5 and RCP8.5 scenarios, and the inter- and intra-annual variability of runoff increased. However, the statistical downscaling of NEX-GDDP is based on Princeton University's global dataset of meteorological forcing (Sheffield et al., 2006), which is less accurate in China than the China meteorological forcing dataset (CMFD) (He et al., 2020), and it lacks the wind speed variables necessary to drive the VIC model. Wang et al. (2019) used three downscaled CMIP5 GCMs data that were based on the Equidistant Cumulative Distribution Function method (EDCDFm) to drive the VIC model, found that EDCDFm could better capture the extremes and spatial distribution of climate elements, and under the RCP4.5 and RCP8.5 scenarios, projected a slight increase in precipitation slightly increase and runoff increase in the upper Yangtze River Basin in the near future (2010–2039) and mid future (2040–2069), exceeding 95%, and in the far future (2070–2099), exceeding 78%. Sun et al. (2019) used 10 CMIP5 GCMs statistically downscaled data based on the observation data from China Meteorological Administration to drive the SWAT model (Arnold et al., 2012) and found that under the RCP4.5 and RCP8.5 scenarios, future precipitation and runoff project increased in the Yangtze River Basin. However, the future scenarios of these studies are RCPs, and the latest SSP scenarios considering socioeconomic development are not used. Yao et al. (2021) used statistically downscaled CMIP6 GCMs data based on CMFD to drive the VIC model, and found that the precipitation in the Huai River Basin is projected to increase in the future, the interannual variation in evapotranspiration and the seasonal variation in runoff are similar to the corresponding time scale variation in precipitation; however, its statistical downscaling method is a simpler linear scaling, and the correlation between the corrected variables and the measured values is weak.

Some scholars have also conducted national-scale studies of future hydrological changes. The results of Cook et al. (2020) based on the CMIP6 multi-GCM ensemble mean showed that under the SSP2-4.5 and SSP5-8.5 scenarios, annual precipitation projected increase in the vast majority of China in 2071–2100 relative to 1985–2014, and the runoff increased significantly in northern China; but they used coarse-resolution runoff from the GCMs themselves and performed only national-scale analyses. Gu et al. (2020) used 31 CMIP5 GCMs and four medium- and small-scale hydrological models to project future runoff changes in 151 small- and medium-sized basins in China, found that relative to 1961–2005, most GCMs project a reduction in annual runoff depth in the upper and middle Yellow River, upper Yangtze River, Heilongjiang River, Pearl River, and Southeastern River basins in 2011–2055 and 2056–2100 under the RCP8.5 scenario; however, this study does not give the macroscopic variation in runoff at the first-level basin scale in China. Based on five downscaled CMIP5 GCMs data from the Inter-Sectoral Impact Model Intercomparison Project (ISIMIP) (Warszawski et al., 2014) and VIC model, Leng et al. (2015) showed that the annual

runoff depths in 1971–2099 were reduced under the RCP8.5 scenario in the Chinese mainland and most basins, using 1971–2000 as the baseline period; but the ISIMIP bias correction for the GCMs was based on a global reanalysis dataset (Frieler et al., 2017; Cucchi et al., 2020), the limited inclusion of Chinese real site observations may lead to bias in the corrected data in China. Therefore, it is still necessary to combine more station observations, adopt a more reasonable statistical downscaling approach, reduce the spatial resolution of projected data, and use the latest and more reliable CMIP6 GCMs and large-scale hydrological models to make more comprehensive and detailed projections and analyses of future basin-scale hydrological changes in China.

In this study, the computationally simpler and more accurate statistical downscaling method EDCDFm (Teutschbein and Seibert, 2012) with the CMFD as the gridded observation reference data was used to downscale six CMIP6 GCMs data for two mid-high warming scenarios, SSP2-4.5 and SSP5-8.5. The downscaled bias-corrected six GCMs data are used to drive the VIC model to simulate the daily and gridded evapotranspiration and runoff depths in China in 1985–2099; using 1985–2014 as the historical baseline period, we analyze the changes in major basins and grid-scale hydrological situations in the 21st century in China relative to the historical period and provide references and comments for future water resource management, drought and flood prevention, and basin-specific responses in China.

2. Materials and methods

2.1 Introduction to the study area

The area of this study is located 73.25°–135.25°E and 18.5°–53.75°N in the Chinese mainland and includes 11 major river basins (Figure 1): the Pearl River (PR), Yangtze River (YZR), Yellow River (YR), Huai River (Huai), Hai River (HR), Yarlung Zangbo River (YZ), Lancang River (LCR), Nujiang River (NR), Hei River (Hei), Liao River (LR), and Songhua River (SR). These basins are divided into southern and northern China: the PR, YZR, Huai, YZ, LCR, and NR are in southern China, and the YR HR, Hei, LR, and SR are in northern China (Leng et al., 2015).

2.2 VIC model and parameter settings

2.2.1 VIC model

The VIC model is a semi-distributed macroscale land surface hydrological model (Liang et al., 1994, 1996), which can simultaneously consider the water balance and energy balance between the land surface and atmosphere and use meteorological data, including precipitation, temperature, wind speed, radiation, humidity and water vapor pressure as forcing, combined with soil parameters, vegetation parameters and other subsurface parameters to simulate evapotranspiration, soil water content, surface runoff depth, baseflow depth, snow water equivalent, etc. As a mature time-step-by-time step, grid-by-grid simulation hydro-

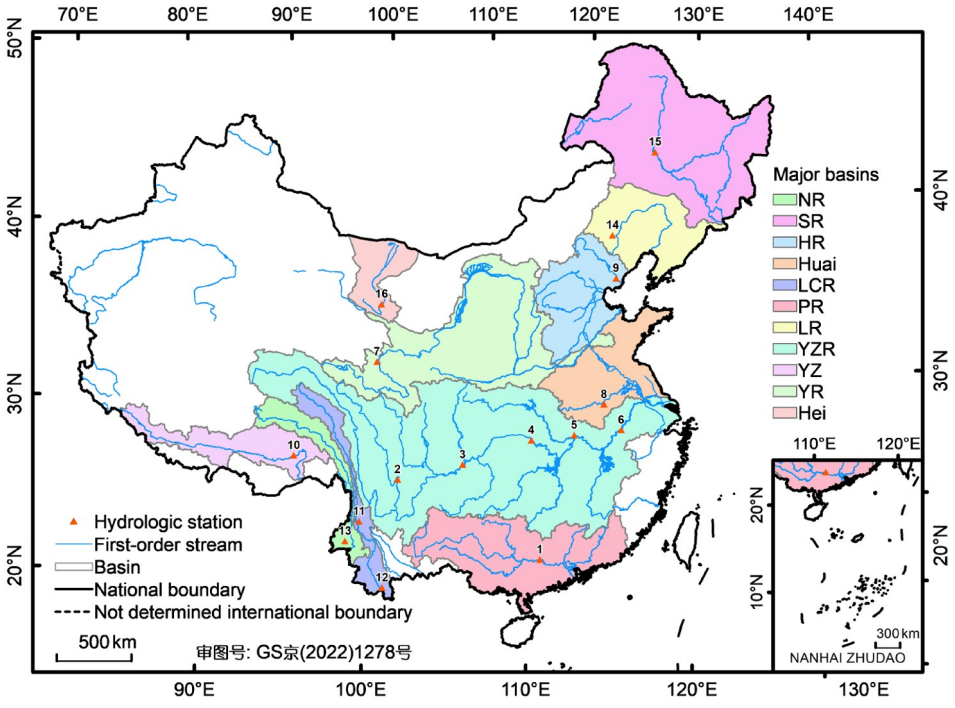

Figure 1 Spatial distribution map of 11 major basins and hydrological stations in the study area. 1, Wuzhou; 2, Luning; 3, Cuntan; 4, Yichang; 5, Hankou; 6, Datong; 7, Tangnaihai; 8, Lutaizi; 9, Luanxian; 10, Nuxia; 11, Jiuzhou; 12, Yunjinghong; 13, Daojieba; 14, Chifeng; 15, Jiangqiao; 16, Yingluoxia.

logical model, the VIC model has been successfully applied in many large and medium-sized basins worldwide (Wu et al., 2017; Liu et al., 2018; Wang et al., 2018; Bohn and Vivoni, 2019; Yang et al., 2019, 2021). The VIC model establishes a set of empirical relationships that can be used to derive radiative variables by daily precipitation, daily maximum temperature, and daily minimum temperature (Liang et al., 1994); it can be enabled to perform water balance calculations only, using four variables: precipitation, maximum temperature, minimum temperature, and wind speed for hydrological simulations when the remaining meteorological or radiative variables are difficult to obtain.

2.2.2 VIC model parameter settings

In this study, VIC model version 4.06 (https://vic.readthedocs.io/en/master/) was used, with a simulated grid size of 0.25° and a time step of one day. The surface cover types in the model soil parameters were obtained from the University of Maryland Global Vegetation Classification dataset (Hansen et al., 2000), and the leaf area index was a climatic state value that varied from month to month (Maurer et al., 2002; Zhang et al., 2014); the shape parameters of the infiltration curve, depth per soil layer, and baseflow parameters were consistent with Zhang et al. (2014). This parameter was calibrated using the natural streamflow at representative hydrological stations in several basins in China and was successfully validated. Since snow and permafrost are not the subjects of interest in this study, only the water balance module of the VIC model is used for hydrology simulation. The daily evapotranspiration (*Evap*), surface runoff (*SurR*) and baseflow (Baseflow) were simulated by four climate variables: precipitation (*P*), near-surface air temperature maximum (T_{max}), near-surface air temperature minimum (T_{min}), and near-surface wind speed (*Wind*). The total runoff (*R*) is obtained by summing the surface runoff and baseflow. In this study, the warm-up period of the VIC model is set to five years (1979–1984), and the simulation period is 1985–2099.

2.2.3 Routing method

In this study, the global hydrodynamic model Catchment-based Macroscale Floodplain (CaMa-Flood) was used for river routing; CaMa-Flood routes input runoff generated by the hydrological model to oceans or inland seas along a prescribed river network map and calculates river and floodplain water storage, river discharge, water depth, and inundated area for each grid point (Yamazaki et al., 2011); it is easy to implement, has more reliable results than other models, and is widely used in flood analysis worldwide (Lim et al., 2018). The CaMa-Flood model grid resolution used in this study is 0.25° with a temporal resolution of one day.

2.3 Model input data

2.3.1 CMFD dataset

The CMFD dataset spans 1979–2018 and includes seven elements: near-surface air temperature, surface pressure, specific humidity, wind speed, downward shortwave radiation, downward longwave radiation and precipitation rate, with a temporal resolution of 3 h and a spatial resolution of 0.1°. Its accuracy for China is better than that of the internationally available reanalysis data (Yang et al., 2010; He et al., 2020). The daily precipitation rate, daily near-surface maximum temperature, daily near-surface minimum temperature, and daily near-surface wind speed of CMFD in 1979–2014 were interpolated to 0.25° by the bilinear interpolation method and as the measured information for the VIC model atmospheric drive and GCM bias correction. Previous studies have shown that wind speed has a small effect on VIC model hydrological simulations (Wu et al., 2011; Wang et al., 2012; Livneh et al., 2013) and that only the precipitation and temperature of GCMs are generally statistically downscaled when studying the impact of future climate change on the water cycle (Wang et al., 2019; Wang et al., 2021); therefore, bias correction for the interpolated wind speed of GCMs was not performed in this study.

2.3.2 GCMs data

The GCMs are a powerful tool used by scientists to simulate Earth's climate change and project future climate change in response to human activities and land, ocean and atmospheric interactions. This study uses the historical scenario data and combined scenarios (SSPs-RCPs) data for different SSPs and RCPs (Eyring et al., 2016) from the latest CMIP6 GCMs (https://esgf-node.llnl.gov/search/cmip6/), as the VIC model atmospheric forcing. Based on the variable's completeness, representativeness, and usage frequency of GCMs at the beginning of the study, six CMIP6 GCMs (CanESM5, FGOALS-g3, GFDL-CM4, IPSL-CM6A-LR, MPI-ESM1-2-HR, and MRI-ESM2-0) data from five countries and different research institutions were used to conduct this study. Detailed information is shown in Table 1. The selected periods are the historical period 1979–2014 and the future period 2015–2099 under two scenarios, SSP2-RCP4.5 (SSP2-4.5) and SSP5-RCP8.5 (SSP5-8.5): the SSP2-4.5 scenario is a combination of middle-of-the-road future forcing SSP2 and RCP4.5 scenarios and reflects future climate changes under nonextreme land use and aerosol scenarios; the SSP5-8.5 scenario is a combination of the higher future forcing SSP5 and RCP5.8 scenarios and accounts for the only scenario among the SSPs that can produce a radiative forcing of 8.5 W m^{-2} in 2100; both scenarios are in the Tier 1 experiments of CMIP6 (O'Neill et al., 2016).

The downscaling methods of GCMs mainly include dy-

Table 1 Basic information of six CMIP6 GCMs

No.	Name	Abbreviation	Nation	Resolution (km)
1	CanESM5	Can	Canada	500
2	FGOALS-g3	FGO	China	250
3	GFDL-CM4	GFDL	U.S.	100
4	IPSL-CM6A-LR	IPSL	U.S.	250
5	MPI-ESM1-2-HR	MPI	Germany	100
6	MRI-ESM2-0	MRI	Japan	100

namic downscaling and statistical downscaling. Although the former has clear physical meaning, it is more computationally intensive, while the latter is relatively easy to calculate and can correct the statistical bias of the GCMs with better results, so it is widely used in research regarding the impact of climate change at the regional scale (Sun et al., 2013; Zhang et al., 2016; Xu and Wang, 2019). Teutschbein and Seibert (2012) used different statistical methods to correct the precipitation and temperature of regional climate models for five mesoscale basins in Switzerland and found that the method based on the cumulative distribution function (*CDF*) was the most effective. Based on this result, Li et al. (2010) proposed the equidistant cumulative distribution function method (EDCDFm), which corrects the *CDF* of the GCM variables to be consistent with the measured data in the historical period, and the GCM output of the future scenario is corrected according to the difference between the *CDF* of the GCMs historical period and the measured data. The study shows that EDCDFm can effectively capture the extreme values of climate elements and improve the accuracy of the GCMs and model simulation after downscaling. Therefore, this study used the EDCDFm method, CMFD and the six GCMs, which were first downscaled (DS) to 0.25° spatial resolution by bilinear interpolation; the daily T_{max}, daily T_{max}, and daily P of each GCM grid were then biased corrected (BC) based on the *CDF* of the corresponding grid series. The *CDF* was calculated by referring to the paper (Watterson, 2008; Li et al., 2010), where the probability density function (*PDF*) of temperature was estimated using a four-parameter beta function, the *PDF* of precipitation was estimated using a mixed gamma distribution function, and the parameters were estimated using the 1979–2014 series for the historical period and the 2015–2100 series for the future period. The calculations of the historical period and future period are shown in eqs. (1) and (2), respectively.

$$x_{\text{m-c,adjust}} = F_{\text{o-c}}^{-1}\left(F_{\text{m-c}}(x_{\text{m-c}})\right), \tag{1}$$

$$x_{\text{m-p,adjust}} = x_{\text{m-p}} + F_{\text{o-c}}^{-1}\left(F_{\text{m-p}}(x_{\text{m-p}})\right) - F_{\text{m-c}}^{-1}\left(F_{\text{m-p}}(x_{\text{m-p}})\right), \tag{2}$$

where $x_{\text{m-c,adjust}}$ and $x_{\text{m-p,adjust}}$ are bias-corrected climate element values for GCMs historical and future periods, respectively; $F_{\text{o-c}}^{-1}$ and $F_{\text{m-c}}^{-1}$ are the quantile functions obeyed for the measured data and GCMs data, respectively; $F_{\text{m-c}}$ and $F_{\text{m-p}}$ are the cumulative distribution functions for GCMs historical and future periods, respectively; $x_{\text{m-c}}$ and $x_{\text{m-p}}$ are the meteorological element values for GCMs historical and future periods, respectively.

Three indicators were used to evaluate the downscaling bias-corrected GCMs data accuracy in monthly values: mean absolute error (*MAE*), root mean squared error (*RMSE*), and Pearson correlation coefficient (*PCC*). The smaller the value of *MAE* and *RMSE* is, the smaller the bias of the GCMs data from the measured value. The value of *PCC* falls between −1 and 1; the closer it is to 1, the stronger the positive correlation is between the GCMs and the measured data, and the closer it is to −1, the stronger the negative correlation is between the GCMs' data and the measured data.

2.4 Streamflow simulation validation

Measured streamflow was used as references to evaluate the monthly simulation performance of the VIC and CaMa-Flood model; these measurements represented 15 hydrological stations in ten major river basins of China based on data from the Ministry of Water Resources and the Yingluoxia hydrological station (Figure 1 and Table 2) in the Hei Basin based on data from the National Tibetan Plateau Data Center (Liu et al., 2016a, 2016b; Xie, 2016). Three error evaluation indicators were used: mean relative error (*MRE*), *PCC* and Nash-Sutcliffe efficiency coefficient (*NSE*) (eq. (3)). Generally, a value of *NSE* closer to 1 indicates that the simulation results are better, and an *NSE* less than 0 indicates that the simulation results are unreliable.

$$NSE = 1 - \frac{\sum_{i=1}^{n}(X_i - S_i)^2}{\sum_{i=1}^{n}\left(X_i - \overline{X}_i\right)^2}, \tag{3}$$

where S_i is the simulated value, X_i is the measured value, and n is the number of months.

3. Results

3.1 Accuracy of model-simulated streamflow

CMFD was applied as the atmospheric forcing; the monthly

Table 2 Detailed information of 16 hydrological stations in China and error evaluation table of the simulated streamflow

No.	Station name	Basin	Location		Basin area (10^3 km^2)	Validation period	*NSE*	*MRE* (%)	*PCC*
			Longitude	Latitude					
1	Wuzhou	PR	111.3°E	23.48°N	310	1984–2009	0.93	15.9	0.97
2	Luning	YZR	101.87°E	28.45°N	108	1984–2008	0.73	28.7	0.96
3	Cuntan	YZR	106.36°E	29.37°N	867	1984–2008	0.86	20.7	0.97
4	Yichang	YZR	111.23°E	30.67°N	1006	1984–2009	0.88	18.7	0.97
5	Hankou	YZR	114.28°E	30.77°N	1488	1984–2009	0.89	13.9	0.97
6	Datong	YZR	117.62°E	30.77°N	171	1984–2008	0.86	15.4	0.96
7	Tangnaihai	YR	100.05°E	35.4°N	122	1984–2009	0.60	43.7	0.91
8	Lutaizi	Huai	116.63°E	32.4°N	88	1984–2008	0.71	38.7	0.92
9	Luanxian	HR	118.75°E	39.73°N	44	1984–2008	0.60	58.8	0.80
10	Nuxia	YZ	94.57°E	29.47°N	191	1984–2008	0.74	37.4	0.89
11	Jiuzhou	LCR	99.38°E	25.83°N	84	1984–2008	0.73	30.7	0.87
12	Yunjinghong	LCR	101.07°E	21.88°N	138	1984–2007	0.69	32.5	0.86
13	Daojieba	NR	98.53°E	24.59°N	115	1984–2007	0.78	27.1	0.91
14	Yingluoxia	Hei	100.18°E	38.82°N	10	1984–2014	0.81	25.1	0.90
15	Chifeng	LR	118.57°E	42.17°N	8.7	1984–2006	0.70	56.1	0.84
16	Jiangqiao	SR	123.68°E	46.78°N	163	1984–2002	0.74	49.8	0.88

hydrographs of the VIC and CaMa-Flood model-simulated and observed streamflow at the hydrological stations are shown in Figure 2. The *NSE* of monthly streamflow between simulations and observations is at or above 0.60 at each station (Table 2), suggesting that the VIC model is more applicable to hydrological simulations in China. The accuracy of the simulated monthly streamflow is best in the PR, YZR and Hei basins, with *NSE*s of 0.90, 0.70–0.80, and above 0.80, respectively. The stations with relatively poor simulation results are mainly located in the YR and HR basins, with *NSE*s of 0.60, which may be related to the fact that YR and HR basins are more influenced by human activities. The *MRE* of simulated monthly streamflow is relatively small in the PR, YZR, Hei, NR and LCR basins, with 15–30%, while it is relatively large in the HR, SR, and YR basins, which may be related to the drier northern region with smaller streamflow and larger human water consumption (Table 2). The *PCC*s between the simulated and measured monthly streamflow at all basin stations are approximately 0.9 except for the HR basin, and in the PR and YZR basins, the *PCC*s are approximately 0.97. In summary, the hydrological station monthly streamflow based on CMFD and VIC model simulations had small errors and strong correlations with the observation streamflow in all basins, and the VIC model and CMFD driver used in this study performed well in the Chinese mainland (Table 2).

3.2 Effects of GCMs data downscaling bias correction

3.2.1 GCMs data accuracy changes in the historical period

After downscaling bias correction, the GCMs for the historical period (1985–2014) and the CMFD multiyear average monthly precipitation (*P*), monthly mean daily maximum (T_{max}), and minimum (T_{min}) temperature are consistent in spatial distribution (Appendix Figures S1–S3, link.springer.com), and the *RMSE* of T_{max} and T_{min} are below 3°C month^{-1} for most of the grids. The *RMSE* of *P* is basically in the range of 2–180 mm month^{-1}, decreasing gradually from the southeast coast to the northwest inland (Appendix Figures S4–S6). The grid *MAE*s of *P*, T_{max}, and T_{min} before (DS) and after (BC) downscaling bias correction for each GCM data are shown in Figure 3. After bias correction, the *MAE*s of the three variables for single GCM data are 0.4–4.6 mm month^{-1}, 0.06–0.1°C month^{-1}, and 0.06–0.08°C month^{-1}, respectively, which are much smaller than those before bias correction of 18.3–28.8 mm month^{-1}, 1.7–3.3°C month^{-1}, and 2.0–4.3°C month^{-1} (Figure 3a). After bias correction, the RMSEs of *P*, T_{max}, and T_{min} are 48.7–65.6 mm month^{-1}, 2.1–3.0°C month^{-1}, and 2.0–2.7°C month^{-1}, respectively, which are also much smaller than those before bias correction of 54.7–74.0 mm month^{-1}, 3.5–5.0°C month^{-1}, and 3.5–5.8°C month^{-1} (Figure 3b). The *PCC*s of *P*, T_{max}, and T_{min} with CMFD for each GCM before bias correction are 0.51–0.82, 0.89–0.94, and 0.88–0.95, respectively, while the *PCC*s of the variables after bias correction are all above 0.99 (Figure 3c).

By combining the above indicators, after bias correction, the *MAE* and *RMSE* of monthly *P*, T_{max}, and T_{min} of each GCM are substantially reduced, *PCC* is close to 1, and EDCDFm is better for bias correction of the six GCMs' daily *P*, T_{max}, and T_{min}.

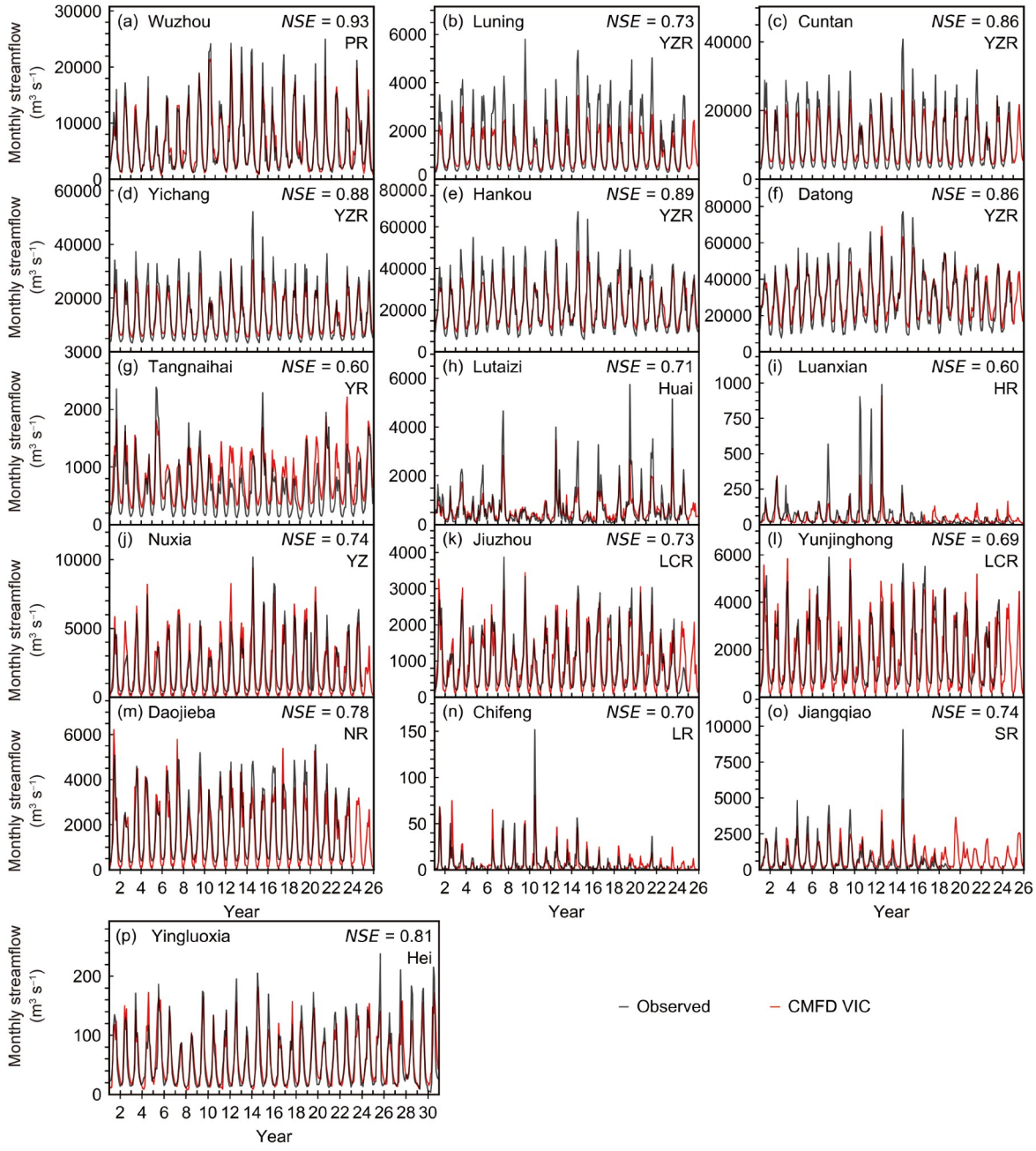

Figure 2 Comparison of simulated and measured monthly streamflow at each hydrological station in 1984–2009 ((p) Yingluoxia station in 1984–2014).

3.2.2 GCMs Simulation accuracy in the historical period

Because different basins have different climatic conditions, underlying surface circumstances, and socioeconomic development levels, the result of six GCMs arithmetic ensemble mean (Ensemble) before (DS) and after (BS) statistical downscaling bias correction is compared with CMFD-based annual P, annual evapotranspiration (E), and annual runoff depth (R) for each basin in the historical period (1985–2014). The effect of statistical downscaling on GCMs and hydrological simulations and the confidence of GCM simulation results in the historical period can thus be analyzed (Figure 4).

As seen from Figure 4, after bias correction, the annual P, annual E, and annual R based on GCM Ensemble are closer to the measured values, and the errors relative to CMFD variables are reduced in most of the basins, with the largest reduction in the errors of P and R in the YZ (Figure 4h) basin, at −160% and −200%, respectively. For single basins, the annual P from GCM Ensemble is slightly overestimated in most basins, with smaller underestimates (<3 mm) in the HR (Figure 4e), LR (Figure 4f), and Hei (Figure 4k) basins. The annual E based on GCM Ensemble is similar to the measured

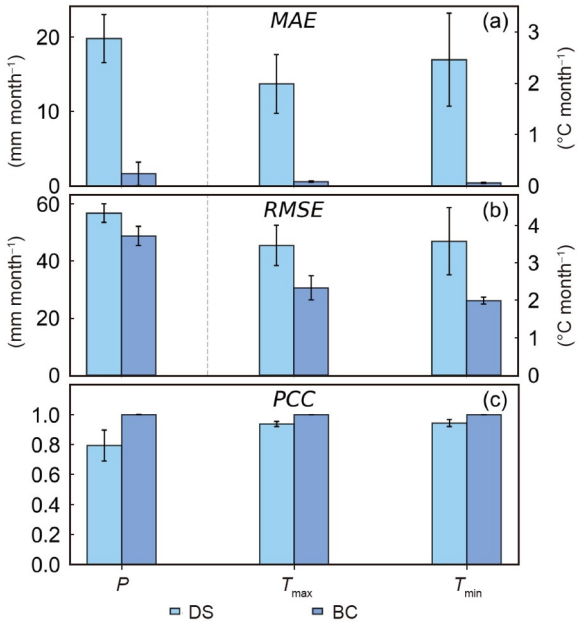

Figure 3 Histogram comparing the multiyear average monthly precipitation (P), monthly mean daily maximum (T_{max}) and minimum (T_{min}) temperatures relative to CMFD error indicator values before (DS) and after (BC) bias correction for GCMs data statistical downscaling from 1979 to 2014. (a)–(c) represent *MAE*, *RMSE*, and *PCC*, respectively, and the error line is 1 standard deviation of the six GCMs data.

value in the Hei (Figure 4k) and YR (Figure 4c) basins, with some underestimation in the Huai (Figure 4d) basin and some overestimation in other basins. The annual R based on GCM Ensemble is somewhat overestimated in the Huai (Figure 4d) basin and slightly underestimated in the LR (Figure 4f), SR (Figure 4g), YZ (Figure 4h), NR (Figure 4i), and LCR (Figure 4j) basins. For the Chinese mainland average, the annual P and annual E based on the GCM Ensemble are slightly overestimated, and the annual R is slightly underestimated (Figure 4l). Overall, after statistical downscaling bias correction, errors of annual P, annual E, and annual R based on the GCM Ensemble are substantially reduced over the historical period, and the GCM-driven multiyear average hydrologic simulations are more reliable (Figure 4)

3.2.3 *GCMs data variation in the future period*

The comparison of the multiyear average annual P, annual daily maximum T_{max} and minimum T_{min} temperature under the SSP2-4.5 scenario for each GCM before (DS) and after (BC) downscaling bias correction is shown in Figures 5–7, respectively, with the Chinese mainland and each basin as one unit and both the near future (2020–2049) and far future (2070–2099) included. After bias correction, the P in the future period of the GCMs changes greatly and decreases in most of the basins, among which the FGOALS-g3 model has a greater decrease in the P in the YZ basin (Figure 5). After bias correction, the changes in T_{max} and T_{min} are small and increase in most of the

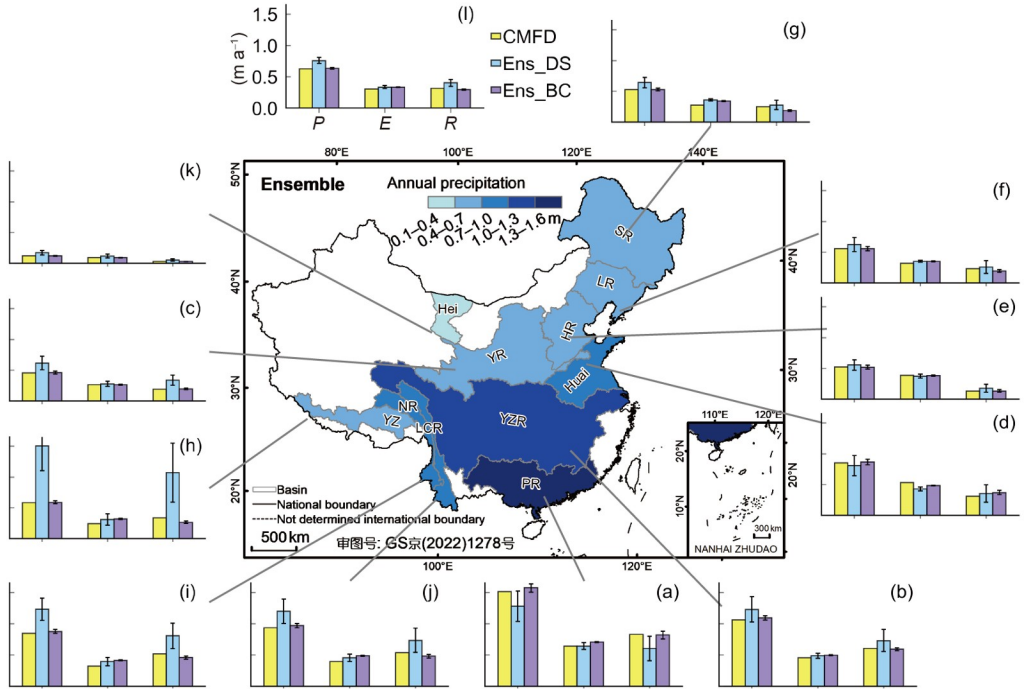

Figure 4 Multiyear average annual precipitation (P), annual evapotranspiration (E), and annual total runoff depth (R) of the basins in the historical period (1985–2014) based on CMFD (yellow) and GCM Ensemble (Ens), before (DS, blue) and after (BC, purple) bias correction, with error lines of 1 standard deviation of the six GCMs data. (a)–(l) represent the following basins: PR, YZR, YR, Huai, HR, LR, SR, YZ, NR, LCR, Hei, and the Chinese mainland, respectively; the coordinate axes of (a)–(k) are the same as those in (l). The color shades of the basins represent the magnitude of the multiyear average P in the historical period.

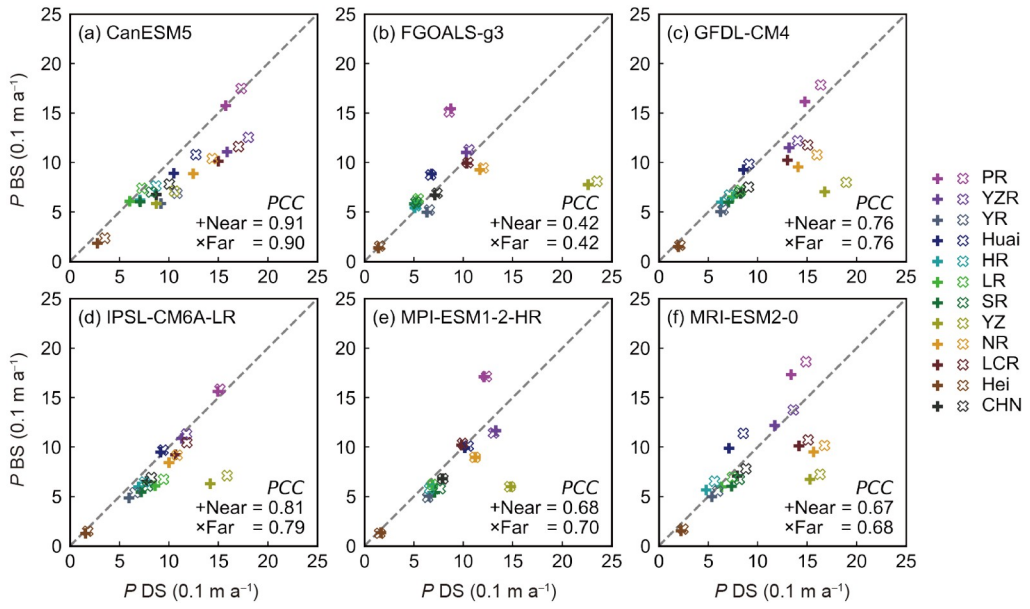

Figure 5 Scatter plots of multiyear average annual precipitation (*P*) before and after downscaling bias correction for each GCM data under the SSP2-4.5 scenario. "+" indicates the near future (2020–2049), "×" indicates the far future (2070–2099), different colors represent different basins, and CHN means the Chinese mainland. *PCC* is the correlation coefficient of each model before (DS) and after (BC) downscaling bias correction.

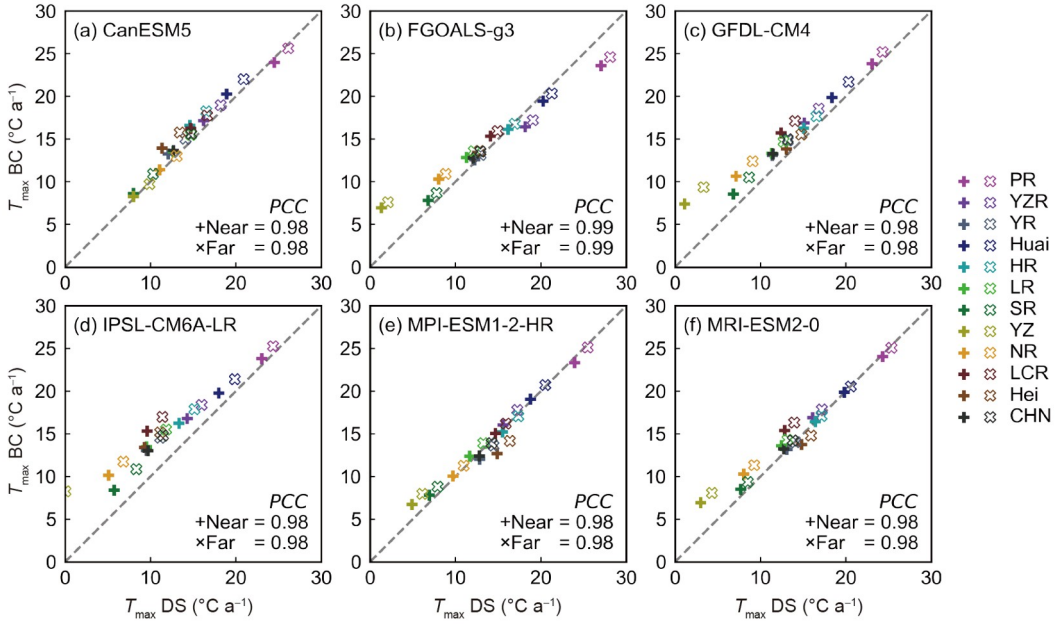

Figure 6 The symbols mean the same as in Figure 5, but the variable is the multiyear average daily maximum temperature (T_{max}).

basins, but the T_{max} in the PR, Huai and YZR basins of the FGOALS-g3 model (Figure 6) and the T_{min} in the Hei Basin of the GFDL-CM4, MPI-ESM2-0, and MRI-ESM2-0 models decrease (Figure 7). The relative changes in the GCMs in each unit after downscaling bias correction under the SSP5-8.5 scenario are similar to those under the SSP2-4.5 scenario, as detailed in Appendix Figures S7–S9.

3.3 Hydrological process variation

3.3.1 Time variation analysis

To reflect the variation in hydrological variables in annual totals over time during the study period, this paper plots the spatially mean 1985–2099 annual *P*, annual *E*, and annual *R* hydrographs for the Chinese mainland (Figure 8 and Appendix Figure S10). As seen from Figure 8, the annual var-

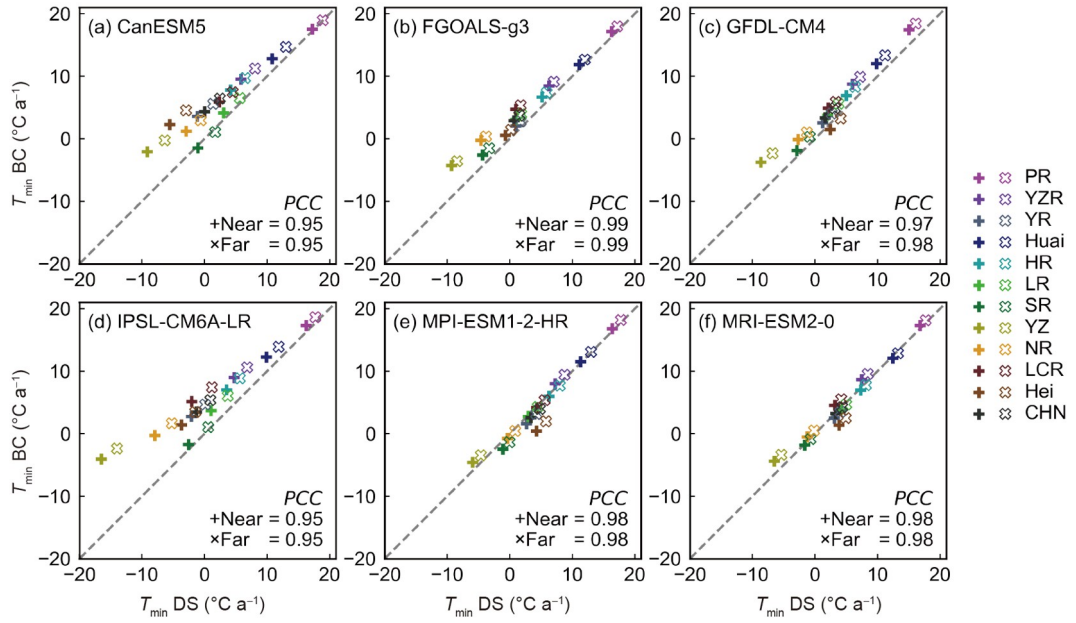

Figure 7 The symbols mean the same as in Figure 5, but the variable is the multiyear average daily minimum temperature (T_{min}).

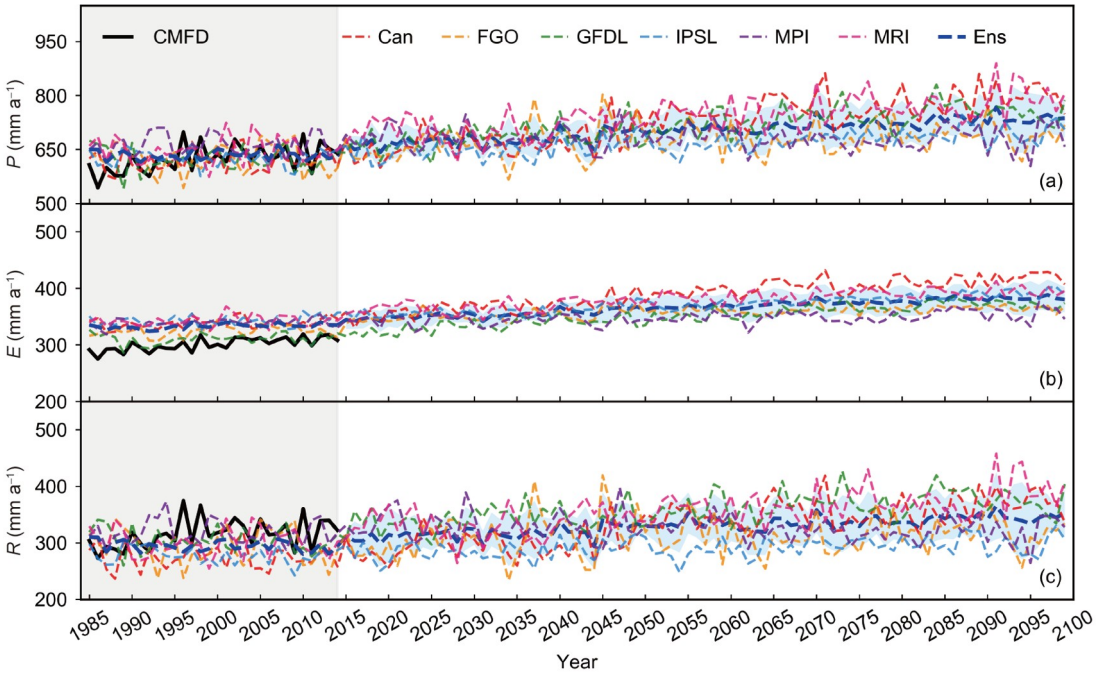

Figure 8 Average annual precipitation (*P*), evapotranspiration (*E*), and runoff depth (*R*) change hydrograph for the Chinese mainland in 1985–2099 when the future scenario is SSP2-4.5; the solid line is the CMFD value, the thin dashed line is the simulated value of each model, the thick blue dashed line is the multi-GCM Ensemble (Ens) value, and the shaded area indicates 1 standard deviation of six GCMs data.

iation in hydrologic variables is large for the single GCM during the historical period, the GCM Ensemble reflects relatively gentle hydrologic variability, and the simulated annual *P* (Figure 8a), annual *E* (Figure 8b), and annual *R* (Figure 8c) in 2014 are approximately 630, 335, and 295 mm, respectively. In the future period (2015–2099) under the SSP2-4.5 scenario, the annual *P* (Figure 8a), annual *E* (Figure 8b), and annual *R* (Figure 8c) projected by the GCM Ensemble wavelike rise from approximately 670, 345, and 310 mm to approximately 740, 380, and 350 mm, respectively, and change more dramatically under the SSP5-8.5 scenario (Appendix Figure S10). The annual *P* (Appendix Figure S10a), annual *E* (Appendix Figure S10b), and annual *R* (Appendix Figure S10c) projected by the GCM Ensemble

wavelike rise from approximately 680, 345, and 320 mm to 810, 425, and 370 mm, respectively. The range of variation in hydrologic variables and inter-GCM standard deviation of single GCM projections also increased with the prediction period, and the uncertainty of the multi-GCM Ensemble increased.

3.3.2 *Spatial variation analysis*

To analyze the spatial distribution of climate change and hydrologic variability, this study draws the spatial distribution map of multiyear averages of annual *P* (Figure 9a0), annual *E* (Figure 9b0), and annual *R* (Figure 9c0) for the historical period (1985–2014) based on CMFD and the GCM Ensemble under the SSP2-4.5 scenario (Figure 9) and SSP5-8.5 scenario (Appendix Figure S11) and the spatial distribution map of the change rate (*CR*) of multiyear average hydrologic variables relative to the historical period in the near future (2020–2049) and the far future (2070–2099).

As seen from Figure 9, the multiyear average of hydrological variables for the historical period in the Chinese mainland all decreased from southeast to northwest (Figure 9a0–c0), with annual *P* above 100 mm in most of the northwest (<100 mm in Tarim Basin) and approximately 1000–3000 mm in the southeast (Figure 9a0), while annual *E* and annual *P* were basically less than 50 mm in the northwest, and in the southeast were approximately 250–1500 and 1000–2500 mm, respectively. In the southeast, the multiyear average annual *E* is generally smaller than the annual *R*, while in the north and southwest, the multiyear average annual *E* is generally larger than the annual *R* (Figure 9b0, 9c0).

Under the SSP2-4.5 scenario, the near future multiyear average annual *P* increases in most of China relative to the historical period but decreases in northern Yunnan (Figure 9a1). The annual *E* only decreases in the northern Xinjiang region but increases in all other regions and the increasing trend is greater in the northwest than in the southeast, with the largest increase in the northeast corner of the Qinghai-Xizang Plateau (Figure 9b1). The annual *R* shows decreasing

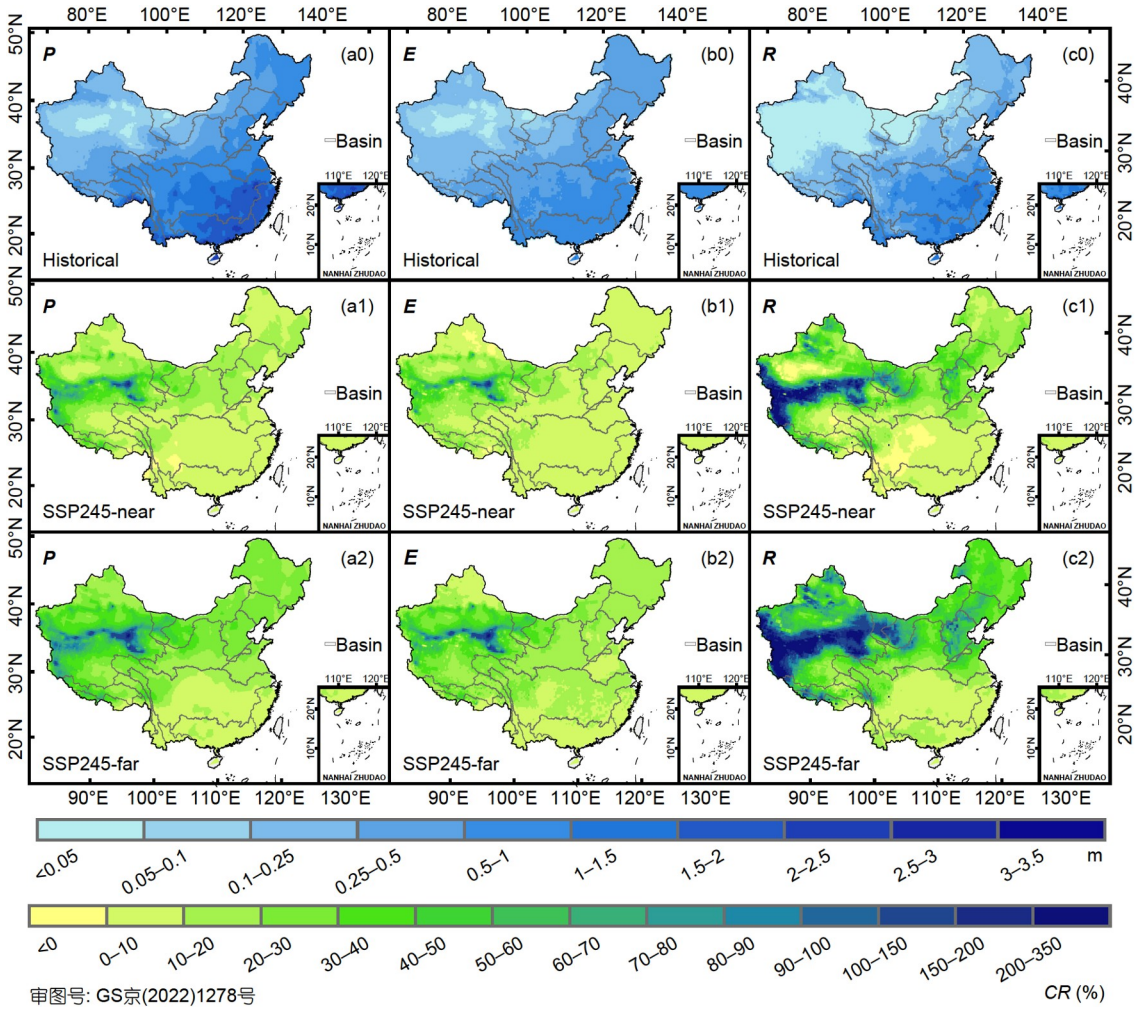

Figure 9 The change rates (*CR*) of the multiyear average annual precipitation (*P*), annual evapotranspiration (*E*), and annual total runoff depth (*R*) of the GCM Ensemble in future periods under the SSP2-4.5 scenario relative to the historical period. (a)–(c) represent *P*, *E*, and *R*, respectively, and numbers 0–2 represent the historical period (Historical), the near future (SSP245-near), and the far future (SSP245-far), respectively.

changes in the Tarim Basin, the southern southwestern river basin and the upper YZR basin but increases in all other regions, particularly in the HR, YR, and Hei basins in northern China, with *CR*s up to 150% near the Tarim Basin and Qinghai-Xizang Plateau boundary (Figure 9c1); the *CR*s of annual *R* and annual *P* have some spatial correlation (Figure 9a1, 9c1). In the far future, the multiyear average annual *P* of all grids in the Chinese mainland mostly increases, and the *CR* between the south and the north is bounded by ~10%, showing a distribution pattern of larger in the north and smaller in the south (Figure 9a2). The increase in annual *E* is relatively small in the Huai and PR basins, while the relatively large increase occurs in the northwest, especially at the northern boundary of the Qinghai-Xizang Plateau, where the relative *CR* exceeds 70% (Figure 9b2). The spatial distribution of the relative *CR* of annual *R* remains similar to that of annual *P* (Figure 9a2, 9c2) and increases basically in all the Chinese mainland grids, but the 10% *CR* dividing line moves south to the northern YZR basin; in the northern Qinghai-Xizang Plateau, the relative *CR* is as high as 80% (Figure 9c2). The dramatic changes in future projected hydrological variables near the northern boundary of the Qinghai-Xizang Plateau may be related to the small *P*, *E*, and *R* during the historical baseline period in the region, resulting in a larger relative CR due to the same hydrologic changes.

The spatial distributions of the multiyear average annual *P*, annual *E*, and annual *R* relative to the historical period CR under the SSP5-8.5 scenario (Appendix Figure S11) for the near future (Appendix Figure S11a1–c1) and far future (Appendix Figure S11a2–c2) are similar to those for the SSP2-4.5 scenario, but the SSP5-8.5 scenario has more drastic changes. More areas experience relative decreases in annual *P* in the near future (Appendix Figure S11a1), fewer areas experience relative decreases in annual *R* (Appendix Figure S11c1), and some areas of the upper southwestern YZR experience decreases in the annual *R* in the far future relative to the historical period (Appendix Figure S11c2), which may be related to the higher future radiative forcing assumptions in the SSP5-8.5 scenario.

3.3.3 *Temporal variation in the basins*

To study the future changes in hydrology relative to the historical period (1985–2014) for the Chinese mainland and major basins under the SSP2-4.5 and SSP5-8.5 scenarios, this paper draws the relative CRs in the multiyear average annual *P*, annual *E*, and annual *R* for the GCM Ensemble in the near future (2020–2049) (Figure 10) and the far future

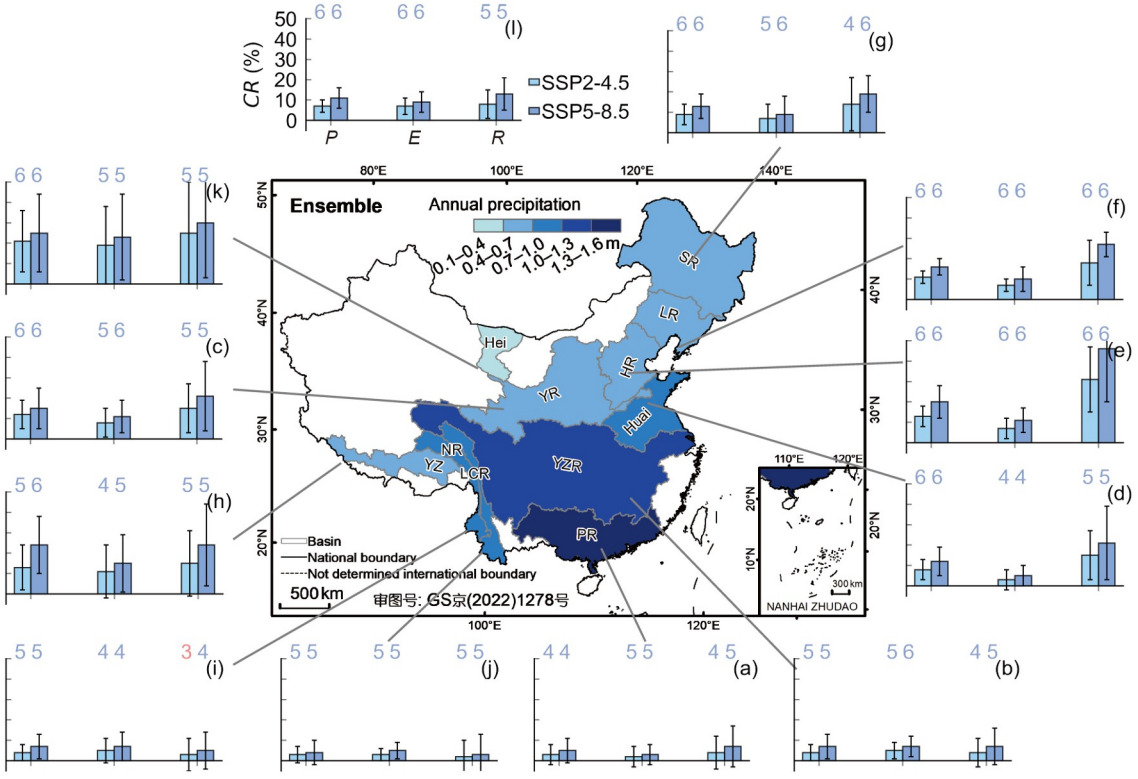

Figure 10 The bias-corrected GCM Ensemble for the near future (2020–2049) multiyear average annual precipitation (*P*), annual evapotranspiration (*E*), and annual total runoff depth (*R*) change rates (*CR*) of the basins relative to the historical period (1985–2014), with error lines of 1 standard deviation for the six GCMs data. The number above the bar indicates the number of models with the same positive or negative *CR* of the variable as the Ensemble; the number not exceeding half of the total number of the models (<4) is red; otherwise, it is blue. (a)–(l) represent the following basins: PR, YZR, YR, Huai, HR, LR, SR, YZ, NR, LCR, Hei, and the Chinese mainland, respectively; the coordinate axes of (a)–(k) are the same as in (l). The color shades of the basins represent the magnitude of the multiyear average *P* in the historical period.

(2070–2099) (Figure 11), in which the Chinese mainland and each basin, which functions as a single unit with a unique spatially averaged variation is calculated (the heatmap of the single GCM and GCM Ensemble *CR* in each unit relative to the historical period is shown in Appendix Figure S12).

For the near future period in the Chinese mainland and the basins, the GCM Ensemble projects increase in multiyear average annual *P*, annual *E*, and annual *R* under the SSP2-4.5 scenario relative to the historical period (Figure 10). The maximum *CR* in annual *E* and the minimum *CR* in annual *R* are shown in the YZR (Figure 10b), NR (Figure 10i), and LCR (Figure 10j) basins, while the maximum *CR* in annual *R* and the minimum *CR* in annual *E* are shown in the other basins and the Chinese mainland. Focusing on the analysis of *R*, the future increases in annual *R* in the near future are small (<10%) in the PR (Figure 10a), YZR (Figure 10b), NR (Figure 10i), and LCR (Figure 10j) basins, and increases in annual *R* in the YR (Figure 10c), Huai (Figure 10d), LR (Figure 10f), SR (Figure 10g), and YZ (Figure 10h) basins are approximately 10–20%. The GCM Ensemble projected that the multiyear average annual *P*, annual *E*, and annual *R* also increased relative to the historical period under the SSP5-8.5 scenario, and the CR was higher than that of the SSP2-4.5 scenario (Figure 10). The multiyear average annual *R* in the Chinese mainland (Figure 10l) increased by more than 10% relative to the historical period. The annual *R* of the YR (Figure 10c), Huai (Figure 10d), and YZ (Figure 10h) basins increased by approximately 20% relative to the historical period, the relative CR in the annual *R* of the LR (Figure 10f) basin was greater than 25%, and the relative CR in the annual *R* in the Hei (Figure 10k) and HR (Figure 10e) basins were as high as 30% and 46%, respectively. The inter-GCM standard deviations of the variables were the largest for annual *R* and the smallest for annual *E* (Figure 10), which shows that the projection of *R* has relatively large uncertainty. In most basins and scenarios, most (>3) GCMs projected positive and negative CR for the three variables in the near future (Figure 10) in agreement with the GCM Ensemble; however, only three GCMs projected an increase in annual *R* in the NR (Figure 10i) basin relative to the historical period under the SSP2-4.5 scenario.

In the far future, the multiyear average annual *P*, annual *E*, and annual *R* projected by the GCM Ensemble under the SSP2-4.5 scenario also increase in the Chinese mainland and the basins relative to the historical period (Figure 11), the *CR* is approximately 1–2 times that of the near future (Figure 10), and the *CR* for all three variables is approximately 15% in the Chinese mainland (Figure 11l). The PR (Figure 11a), and YZR (Figure 11b) basins experience the maximum *CR* in annual *R* and the minimum *CR* in annual *E*, while the other basins and the Chinese mainland experience the maximum *CR* in annual *E* and the minimum *CR* in annual *R*, which is roughly opposite to the distribution of *CR* in the near future (Figure 10). Focusing on *R*, the increase in annual *R* is re-

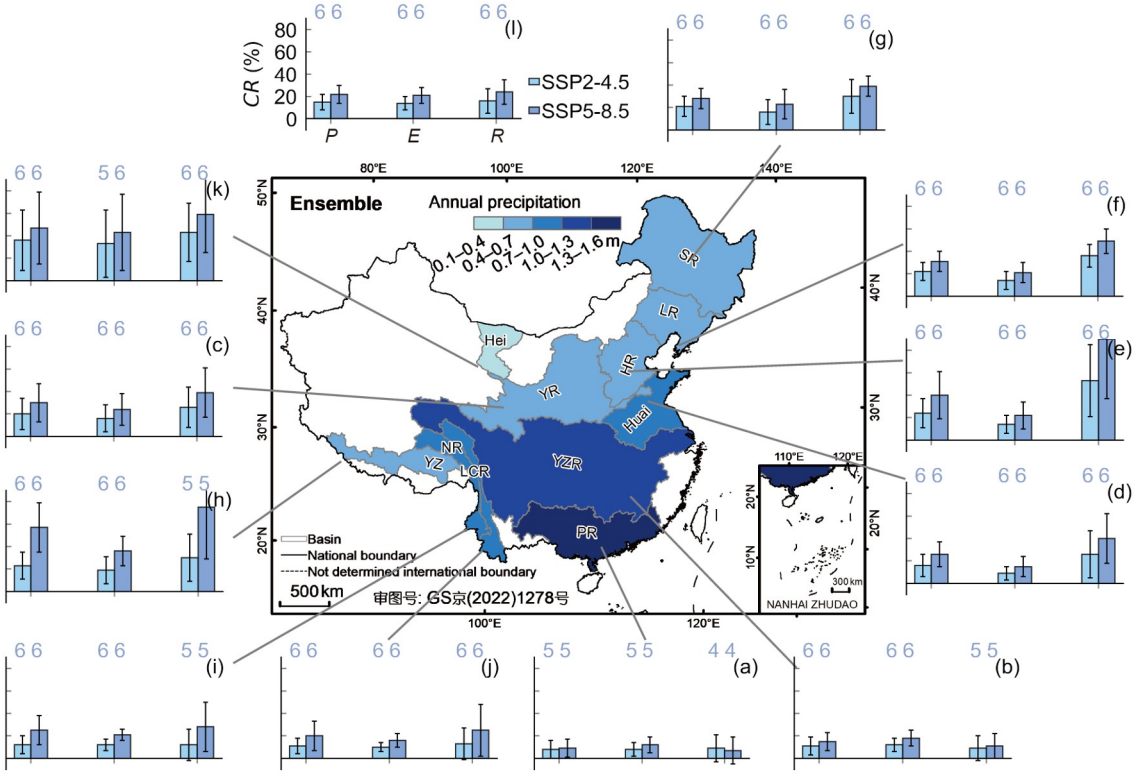

Figure 11 The symbols are the same as in Figure 10, but for the far future (2070–2099).

latively small (<10%) in the PR (Figure 11a) and YZR (Figure 11b) basins, followed by the NR (Figure 11i) and LCR (Figure 11j) basins with a relative CR of 10–15%, while the annual *R* in the YR (Figure 11c), Huai (Figure 11d), SR (Figure 11g), and YZ (Figure 11h) basins increased more by 20–30%. The relative *CR* in annual *R* in the LR (Figure 11f), Hei (Figure 11k), and HR (Figure 11e) basins reached approximately 35%, 40%, and 50%, respectively. Under the SSP5-8.5 scenario, the multiyear average annual *P*, annual *E*, and annual *R* in the Chinese mainland (Figure 11l) projected by the GCM Ensemble increase by approximately 20% relative to the historical period, and the *CR* of hydrological variables relative to the historical period is greater than that of the SSP2-4.5 scenario for all basins and the Chinese mainland except for the PR (Figure 11a) basin, where the relative increase in annual *R* is less than that of the SSP2-4.5 scenario. The GCM Ensemble projects approximately 49%, 59%, 75%, and 90% increases in annual *R* in the LR (Figure 11f), Hei (Figure 11k), YZ (Figure 11h), and HR (Figure 11e) basins, respectively. The inter-GCM standard deviations of the variables were the largest for annual *R* and the smallest for annual *E* (Figure 11), which is the same as those in the near future (Figure 10), demonstrating the relatively large uncertainty in the projection of *R*. Under the SSP2-4.5 and SSP5-8.5 scenarios, most (>3) models in the Chinese mainland and each basin projected the same positive and negative *CR* of the three variables in the far future (Figure 11) as the GCM Ensemble, and the increase in annual *R* in the far future (Figure 11) was more likely than in the near future (Figure 10).

4. Discussion

4.1 Future hydrological changes based on CMIP6

Under the SSP2-4.5 and SSP5-8.5 scenarios, the results of the GCM Ensemble based on the arithmetic ensemble mean of the six CMIP6 GCMs data indicate that the multiyear average annual precipitation (*P*), annual surface runoff depth (*SurR*), and annual total runoff depth (*R*) increase relative to the historical period in most of China in the near and far future (Figure 12). The projected results in the far future (Figure 12a2–c2, 12a4–c4) were compared with the results of the CMIP6 multi-GCM Ensemble (Cook et al., 2020), which was based on the same historical period, future scenarios and similar far future (2071–2100), found that in this study, under both the SSP2-4.5 and SSP5-8.5 scenarios, the annual *P* increases over most of the Chinese mainland, and the increase is larger (>60%) near the boundary between the Tarim Basin and the Qinghai-Xizang Plateau (Figure 12a2, 12a4). The annual *SurR* decreases by approximately 10% in the southeastern Qinghai-Xizang Plateau (Figure 12b2, 12b4). The projected increases in the annual *SurR* and annual *R* in northern China under the SSP5-8.5 scenario are more dramatic than those under the SSP2-4.5 scenario (Figures 12b2, 12c2, 12b4, 12c4), but are all generally consistent with the results in Cook et al. (2020); however, the *CR*s relative to the historical period are generally greater than the results in Cook et al. (2020), which may be related to the higher spatial resolution of the CMIP6 GCMs with statistical downscaling in this paper thus can reveal more details of hydrological spatial variation. Meanwhile, Cook et al. (2020) did not analyze changes in the annual R of southern China in the near future (Figure 12a1–c1, 12a3–c3) and basin-scale hydrological variables relative to the historical period. This study shows that the future projected annual *R* increases in most of southern China relative to the historical period under the SSP2-4.5 and SSP5-8.5 scenarios, but the projected annual *R* decreases in some areas of the YZR basin under the SSP5-8.5 scenario.

4.2 Comparison with the CMIP5-based projected results

Under the premise that both use the VIC model to simulate hydrology, the results of this paper can be compared with those based on the CMIP5 GCMs data to explore the impact of the latest CMIP6 GCMs data on the projection of future hydrological changes. Leng et al. (2015)'s simulation results of five CMIP5 GCMs data based on ISIMIP (GFDL-ESM2M, HadGEM2-ES, IPSL-CM5A-LR, MIROC-ESM-CHEM, and NorESM1-M) with the VIC model showed that, when using 1971–2000 as the historical baseline period, the projected future multiyear average annual *R* in the Chinese mainland under the RCP8.5 scenario continues to decrease by up to −15% by the end of the 21st century. In contrast, the results of this study (Figure 13) show that, when using 1985–2014 as the historical baseline period, under the SSP5-8.5 scenario, the projected multiyear average annual *R* for the Chinese mainland continues to increase in the 21st century, with an increase of approximately 24% at the end of the 21st century, and the growth rate increases roughly until 2035 and slows down after 2035 (Figure 13a), which is similar to the change in the multiyear average annual *P* (Figure 13b). Under the SSP5-8.5 scenario, the growth rate of the multiyear average annual *P* relative to the historical period is consistently greater than the annual *E*, thus leading to a continuous increase in the multiyear average annual *R*. As the projected period extends, the standard deviations between different GCMs increase, and the uncertainty of GCM projections increases (Figure 13), which is consistent with the findings of previous studies (Leng et al., 2015).

At the basin scale, projections based on the CMIP5 (ISIMIP) GCMs Ensemble (Leng et al., 2015) show that multiyear average annual *P* continues to increase in the northern basins of China in the 21st century under the RCP8.5 sce-

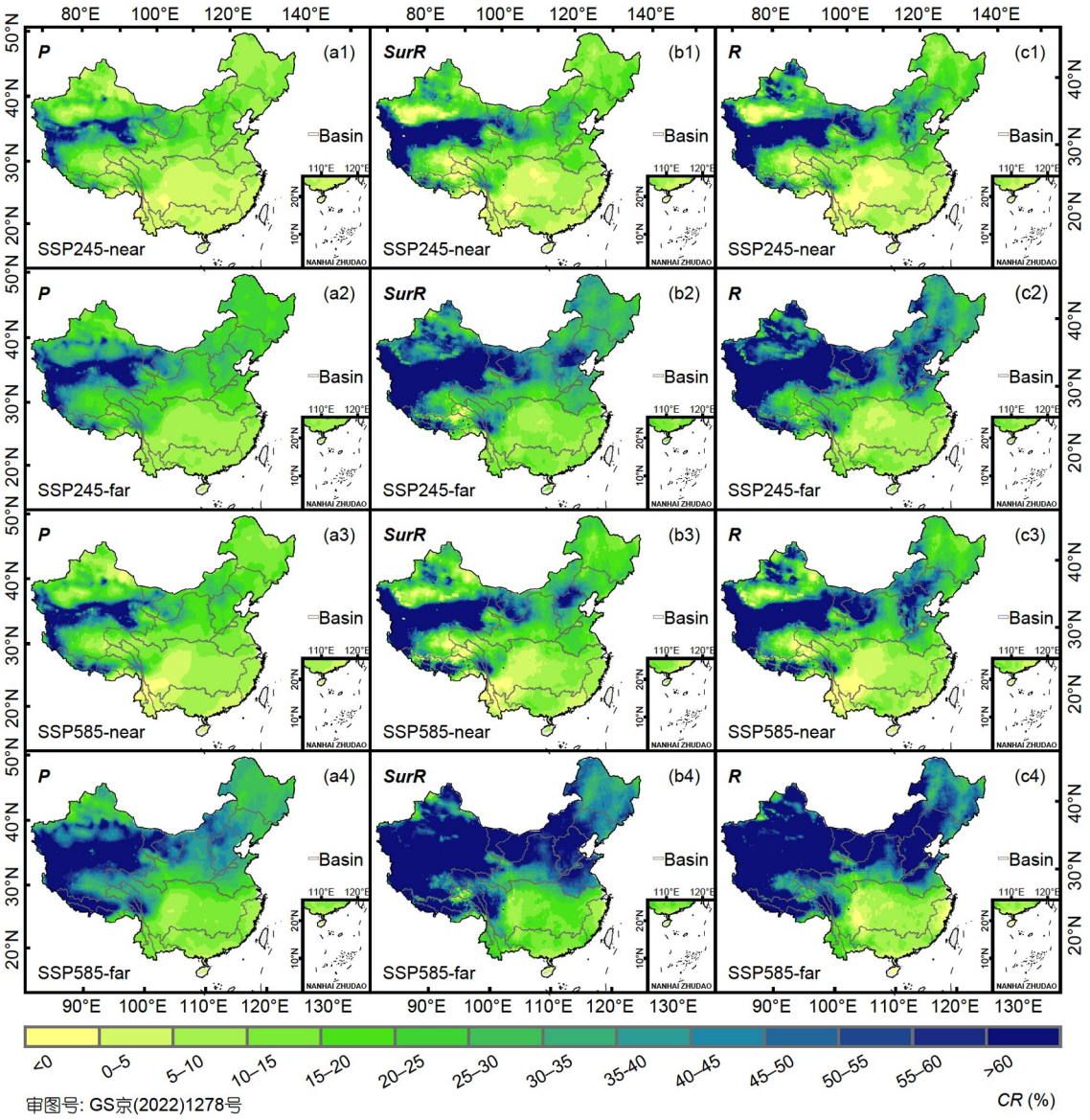

Figure 12 The change rates (*CR*) of the multiyear average annual precipitation (*P*), annual surface runoff depth (*SurR*) and annual total runoff depth (*R*) of the GCM Ensemble in future periods relative to the historical period. (a)–(c) represent *P*, *SurR*, and *R*, respectively. The numbers 1–4 represent four periods: the near future of the SSP2-4.5 scenario (SSP245-near), the far future of the SSP2-4.5 scenario (SSP245-far), the near future of the SSP5-8.5 scenario (SSP585-near), and the far future of the SSP5-8.5 scenario (SSP585-far), respectively.

nario, except for the HR basin, and annual *P* decreases and then increases in the southern basins and the HR basin. Annual *R* continues to decrease in most northern and southern basins in China, with the largest decrease in the YZR basin, which decreases by approximately 25% at the end of the 21st century relative to the historical period, but the LR basin shows a smaller change and the annual *R* in the HR basin shows an increasing trend, with an increase of approximately 15% at the end of the 21st century relative to the historical period. In contrast, the results of this study based on the CMIP6 GCMs show that the multiyear average *P* in both the northern and southern basins of China continues to increase under the SSP5-8.5 scenario, the change in *P* in the northern basin is greater than that in the southern basin, and the change in annual *P* in the YZ basin is relatively the greatest, increasing by approximately 60% at the end of the 21st century relative to the historical period (Figure 14a). The change in annual *R* is similar to that of annual *P* and continues to increase in both southern and northern basins, but the magnitude of change differs from that of annual *P*, with the largest change in annual *R* relative to the historical period in the HR basin, reaching approximately 89% at the end of the 21st century; the YZ basin follows with the next largest change. Moreover, the future multiyear average annual *R* in the YZR and PR basins shows little change relative to the historical period, with relative *CR* stabilizing at ap-

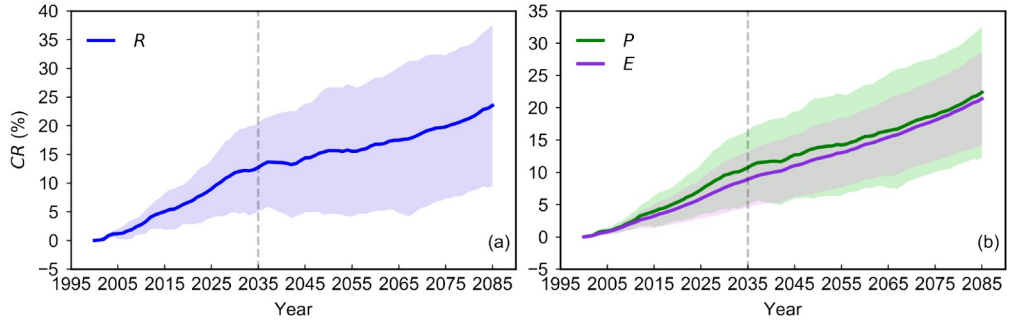

Figure 13 GCM Ensemble *CR* in annual *R* (a) and annual *P* and *E* (b) throughout the 21st century for the Chinese mainland under the SSP5-8.5 scenario. The changes are calculated for every 30-year running average in the time series with respect to 1985–2014. Northern China basins are shown with thin dashed lines, and southern China basins are shown with thick solid lines. Shaded areas indicate 1 standard deviation of the six GCMs data.

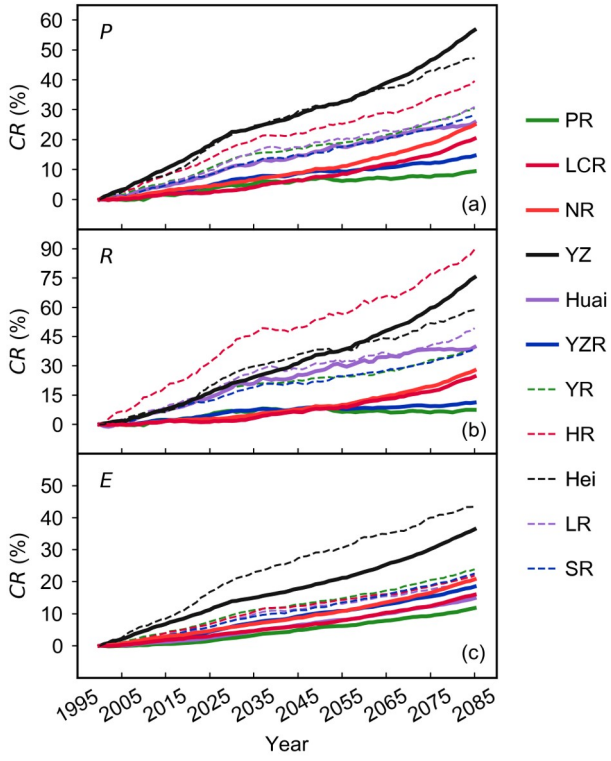

Figure 14 GCM Ensemble CR in annual *P* (a), annual *R* (b), and annual *E* (c) throughout the 21st century for 11 basins in China under the SSP5-8.5 scenario. The changes are calculated for every 30-year running average in the time series with respect to 1985–2014. Northern China basins are shown with thin dashed lines, and southern China basins are shown with thick solid lines.

proximately 10% and 7% in approximately 2030, respectively (Figure 14b). This suggests that future changes in annual *P* using the latest and more reliable CMIP6 GCMs data, considering scenarios of future socioeconomic development, are very different from those considering only future radiative forcing changes, which may be the main reason for the difference in the projected future changes in annual *R*. This study shows that annual *E* increases in all basins relative to the historical period and increases more in the Hei and YZ basins; furthermore, annual *E* changes are greater in the northern basins than in the southern basins (Figure 14c), which is consistent with the results in (Leng et al., 2015).

The results of other scholars based on the VIC model and CMIP5 GCMs data indicate that the future runoff in the YR source region projected increases under the RCP4.5 and RCP8.5 scenarios (Jin et al., 2020), the projected runoff in the upper YZR decreases under the RCP8.5 scenario (Birkinshaw et al., 2017), and projected runoff in the Xijiang River Basin increases under the RCP4.5 and RCP8.5 scenarios (Zhao et al., 2020); however, the areas of the basins they studied are not consistent with the present study, making direct comparisons difficult. The results of studies undertaken by other scholars based on the CMIP6 multi-GCM Ensemble also indicate that under the SSP2-4.5 and SSP5-8.5 scenarios, the future projected precipitation in the LCR basin in the 21st century shows a significant increasing trend (Zhang, 2020); precipitation increase and runoff wavelike rise in the upper Huai Basin (Yao et al., 2021), these findings are consistent with the corresponding results in this paper. More GCMs can be selectively studied in the future (Hassan et al., 2020), and scenarios with low or moderate radiative forcing, such as SSP1-2.6 and SSP3-7.0, can be considered for hydrological change projections in the Chinese mainland (Su et al., 2021).

4.3 Uncertainty in the VIC Model and GCMs Ensemble

Constrained by insufficient measured data, the VIC model used in this study did not calibrate parameters in the western and northwestern basins of China and directly used the calibrated parameters from adjacent basins (Zhang et al., 2014), which would introduce some errors to the streamflow simulation. In terms of climate drivers, the sparseness of the meteorological stations in western China will introduce errors to the CMFD. In terms of model principles, the VIC model tends to perform less well in arid regions than in wet regions (Yang et al., 2019, 2021). These factors create larger uncertainties for the hydrological simulation of the VIC

model in western and northwestern China. Therefore, the basin-scale studies in this paper do not involve basins in western and northwest China where the VIC model parameters are not calibrated, however, the runoff is small in these basins and has little impact on total runoff change at the continental scale in China. In addition, the VIC model used in this study does not consider hydraulic engineering and human water use, which may also introduce some errors to the simulation of streamflow in regions with frequent human activities. In future studies, we intend to collect as much measured meteorological and streamflow data as possible in northwest China, explore the influence and feedback of natural and human factors in the evolution of the terrestrial water cycle (Tang, 2020), and consider for the first time the influence of reservoirs and human activities on streamflow simulations in some regions where data on water conservancy projects and human water use are more complete.

In this paper, the traditional arithmetic ensemble mean analysis method is used for the multi-GCM Ensemble. Recently, the IPCC AR6 has adopted a new method based on observational data with a clear physical meaning of "emergent constraint" (Chen and Lai, 2021) to limit or narrow the range of climate model results. This suggests that the observation constraint can provide new methods and ideas to reduce the uncertainty of multi-GCM prediction, but the "emergent constraint" requires a large number of more reliable observations; more effective and accurate data acquisition can be acquired in the future by using integrated methods of information geography and big data technology (Li et al., 2022).

5. Conclusions

This study, based on the VIC hydrological model, uses six CMIP6 GCMs (CanESM5, FGOALS-g3, GFDL-CM4, IPSL-CM6A-LR, MPI-ESM1-2-HR, and MRI-ESM2-0) data with EDCDFm statistical downscaling bias-corrected and two future scenarios, SSP2-4.5 and SSP5-8.5, to project future changes in the terrestrial surface water cycle in the Chinese mainland and major basins in the 21st century, using CMFD gridded data as a historical reference. The main conclusions are the following three points:

(1) The monthly streamflow simulated by the CMFD-driven VIC model and CaMa-Flood model has *NSE*s of 0.6 in the YR and Huai basins and *NSE*s of 0.7–0.9 in other study basins, indicating that the VIC model hydrological simulation is applicable in the Chinese mainland. The accuracy of 0.25° gridded monthly precipitation, monthly mean daily maximum and minimum temperatures based on CMFD and EDCDFm statistical downscaling bias-corrected is substantially improved in the historical period (1985–2014); the multiyear average annual precipitation, annual evapotranspiration and annual runoff depth based on GCM Ensemble are generally consistent with the results based on CMFD; and the downscaling GCMs are reliable in China. In the near future (2020–2049) and far future (2070–2099), the annual precipitation of each GCM after downscaling bias-corrected decreases substantially in most of the basins, while the annual mean daily maximum and minimum temperatures decrease slightly in most of the basins.

(2) The hydrological projections of the single GCM data at the basin scale have large uncertainties. Under the SSP2-4.5 and SSP5-8.5 scenarios, most of the six GCMs data reflect increases in annual precipitation, annual evapotranspiration, and annual runoff depth in each basin in the near and far future relative to the historical period; however, annual precipitation and annual runoff depth for model MPI-ESM1-2-HR decrease substantially in the YZ, NR, and LCR basins in the near and far future. The annual precipitation and annual runoff depth projected by model IPSL-CM6A-LR decrease in the near future in the NR and LCRiver basins, while model FGOALS-g3 projects a slight decrease in the annual runoff depth in the near future Hei and far future PR basins. The multi-GCM arithmetic ensemble mean reduces the uncertainty of GCM projections.

(3) The annual precipitation, annual evapotranspiration, and annual runoff depth of the GCM Ensemble under the SSP2-4.5 scenario show an overall wavelike rise in 2015–2099 in the Chinese mainland. In the near and far future, the annual precipitation, annual evapotranspiration, and annual runoff depth projected by the GCM Ensemble increase in most of the grids and 11 basins relative to the historical period; the grids with decreasing annual precipitation and annual evapotranspiration in the near future are mainly located in the southwest and northwest regions, respectively, and the grids with decreasing annual runoff depth is mainly distributed in a few regions in the northwest and northwest; in the far future, the annual precipitation, annual evapotranspiration, and annual runoff depth increase in most of the grids in the Chinese mainland. Under the SSP5-8.5 scenario, the annual precipitation, annual evapotranspiration and annual runoff depth projected by the GCM Ensemble also increase in most of the grids, and in the near future is wetter than that under the SSP2-4.5 scenario, and the annual runoff depth in the far future is decreased only in the upper YZR. In other words, under the SSP2-4.5 and SSP5-8.5 scenarios, the future water resources in the Chinese mainland and each basin are likely to increase, and the decrease in annual runoff is likely to occur mainly in the northwest and southwest regions, which can provide a strong scientific reference for future water resource management and risk analysis in China under climate change.

Acknowledgements *The data was supported by the National Qinghai-Tibet Plateau Scientific Data Center (http://data.tpdc.ac.cn) and the*

Earth System Grid Federation (https://esgf-node.llnl.gov/search/cmip6). This work was supported by the Second Tibetan Plateau Scientific Expedition and Research Program (STEP) (Grant No. 2019QZKK0206), the National Key Research and Development Program of China (Grant No. 2017YFA0603703), the National Natural Science Foundation of China (Grant No. 4200011953), and the fundamental scientific research fund of China Institute of Water Resources and Hydropower Research (Grant No. JZ110145B0052021).

References

Ahmed K F, Wang G, Silander J, Wilson A M, Allen J M, Horton R, Anyah R. 2013. Statistical downscaling and bias correction of climate model outputs for climate change impact assessment in the U.S. northeast. Glob Planet Change, 100: 320–332

Arnold J G, Moriasi D N, Gassman P W, Abbaspour K C, White M J, Srinivasan R, Santhi C, Harmel R D, van Griensven A, Van Liew M W, Kannan N, Jha M K. 2012. SWAT: Model use, calibration, and validation. Trans ASABE, 55: 1491–1508

Birkinshaw S J, Guerreiro S B, Nicholson A, Liang Q, Quinn P, Zhang L, He B, Yin J, Fowler H J. 2017. Climate change impacts on Yangtze River discharge at the Three Gorges Dam. Hydrol Earth Syst Sci, 21: 1911–1927

Bohn T J, Vivoni E R. 2019. MOD-LSP, MODIS-based parameters for hydrologic modeling of North American land cover change. Sci Data, 6: 144

Chen D L, Lai H W. 2021. Interpretation of the IPCC AR6 WGI report in terms of its context, structure, and methods (in Chinese). Adv Clim Chang Res, 17: 636–643

Cook B I, Mankin J S, Marvel K, Williams A P, Smerdon J E, Anchukaitis K J. 2020. Twenty-first century drought projections in the CMIP6 forcing scenarios. Earths Future, 8: e2019EF001461

Cucchi M, Weedon G P, Amici A, Bellouin N, Lange S, Müller Schmied H, Hersbach H, Buontempo C. 2020. WFDE5: Bias-adjusted ERA5 reanalysis data for impact studies. Earth Syst Sci Data, 12: 2097–2120

Eyring V, Bony S, Meehl G A, Senior C A, Stevens B, Stouffer R J, Taylor K E. 2016. Overview of the Coupled Model Intercomparison Project Phase 6 (CMIP6) experimental design and organization. Geosci Model Dev, 9: 1937–1958

Frieler K, Lange S, Piontek F, Reyer C P O, Schewe J, Warszawski L, Zhao F, Chini L, Denvil S, Emanuel K, Geiger T, Halladay K, Hurtt G, Mengel M, Murakami D, Ostberg S, Popp A, Riva R, Stevanovic M, Suzuki T, Volkholz J, Burke E, Ciais P, Ebi K, Eddy T D, Elliott J, Galbraith E, Gosling S N, Hattermann F, Hickler T, Hinkel J, Hof C, Huber V, Jägermeyr J, Krysanova V, Marcé R, Müller Schmied H, Mouratiadou I, Pierson D, Tittensor D P, Vautard R, van Vliet M, Biber M F, Betts R A, Bodirsky B L, Deryng D, Frolking S, Jones C D, Lotze H K, Lotze-Campen H, Sahajpal R, Thonicke K, Tian H, Yamagata Y. 2017. Assessing the impacts of 1.5°C global warming—Simulation protocol of the Inter-Sectoral Impact Model Intercomparison Project (ISIMIP2b). Geosci Model Dev, 10: 4321–4345

Gedney N, Cox P M, Betts R A, Boucher O, Huntingford C, Stott P A. 2006. Detection of a direct carbon dioxide effect in continental river runoff records. Nature, 439: 835–838

Gleick P H. 1989. Climate change, hydrology, and water resources. Rev Geophys, 27: 329–344

Gonzalez P, Neilson R P, Lenihan J M, Drapek R J. 2010. Global patterns in the vulnerability of ecosystems to vegetation shifts due to climate change. Glob Ecol Biogeogr, 19: 755–768

Gu L, Chen J, Yin J B, Xu C Y, Zhou J Z. 2020. Responses of precipitation and runoff to climate warming and implications for future drought changes in China. Earths Future, 8: e2020EF001718

Guo S L, Guo J, Hou Y K, Xiong L H, Hong X J. 2015. Prediction of future runoff change based on Budyko hypothesis in Yangtze River Basin. Adv Water Sci, 26: 151–160

Hansen M C, Defries R S, Townshend J R G, Sohlberg R. 2000. Global land cover classification at 1 km spatial resolution using a classification tree approach. Int J Remote Sens, 21: 1331–1364

Hassan I, Kalin R M, White C J, Aladejana J A. 2020. Selection of CMIP5 GCM Ensemble for the projection of spatio-temporal changes in precipitation and temperature over the Niger Delta, Nigeria. Water, 12: 385

He J, Yang K, Tang W, Lu H, Qin J, Chen Y, Li X. 2020. The first high-resolution meteorological forcing dataset for land process studies over China. Sci Data, 7: 25

IPCC. 2021. Climate Change 2021: The Physical Science Basis. Contribution of Working Group I to the Sixth Assessment Report of the Intergovernmental Panel on Climate Change. Cambridge: Cambridge University Press. doi: 10.1017/9781009157896

Jiang D, Hu D, Tian Z, Lang X. 2020. Differences between CMIP6 and CMIP5 models in simulating climate over China and the East Asian Monsoon. Adv Atmos Sci, 37: 1102–1118

Jin J, Wang G, Zhang J, Yang Q, Liu C, Liu Y, Bao Z, He R. 2020. Impacts of climate change on hydrology in the Yellow River source region, China. J Water Clim Change, 11: 916–930

Leng G Y, Tang Q H, Huang M Y, Hong Y, Ruby L L. 2015. Projected changes in mean and interannual variability of surface water over continental China. Sci China Earth Sci, 58: 739–754

Li H B, Sheffield J, Wood E F. 2010. Bias correction of monthly precipitation and temperature fields from Intergovernmental Panel on Climate Change AR4 models using equidistant quantile matching. J Geophys Res, 115: D10101

Li X, Zheng D, Feng M, Chen F. 2022. Information geography: The information revolution reshapes geography. Sci China Earth Sci, 65: 379–382

Liang X, Lettennmaier D P, Wood E F, Burges S J. 1994. A simple hydrologically based model of land surface water and energy fluxes for general circulation models. J Geophys Res-Atmos, 99: 14415–14428

Liang X, Wood E F, Lettenmaier D P. 1996. Surface soil moisture parameterization of the VIC-2L model: Evaluation and modification. Glob Planet Change, 13: 195–206

Lim W H, Yamazaki D, Koirala S, Hirabayashi Y, Kanae S, Dadson S J, Hall J W, Sun F. 2018. Long-term changes in global socioeconomic benefits of flood defenses and residual risk based on CMIP5 climate models. Earths Future, 6: 938–954

Liu M L, Adam J C, Richey A S, Zhu Z C, Myneni R B. 2018. Factors controlling changes in evapotranspiration, runoff, and soil moisture over the conterminous U.S.: Accounting for vegetation dynamics. J Hydrol, 565: 123–137

Liu S, Xie Z H, Zeng Y J. 2016a. Discharge estimation for an ungauged inland river in an arid area related to anthropogenic activities: A case study of Heihe River Basin, Northwestern China. Adv Meteorol, 2016: 1–11

Liu S, Xie Z H, Zeng Y J. 2016b. Estimation of streamflow in ungauged basins using a combined model of black-box model and semi-distributed model-taking Yingluoxia watershed as an example (in Chinese). J Beijing Norm Univ, 52: 393–401

Livneh B, Rosenberg E A, Lin C, Nijssen B, Mishra V, Andreadis K M, Maurer E P, Lettenmaier D P. 2013. A long-term hydrologically based dataset of land surface fluxes and states for the Conterminous United States: Update and extensions. J Clim, 26: 9384–9392

Maurer E P, Wood A W, Adam J C, Lettenmaier D P, Nijssen B. 2002. A long-term hydrologically based dataset of land surface fluxes and states for the Conterminous United States. J Clim, 15: 3237–3251

O'Neill B C, Tebaldi C, van Vuuren D P, Eyring V, Friedlingstein P, Hurtt G, Knutti R, Kriegler E, Lamarque J F, Lowe J, Meehl G A, Moss R, Riahi K, Sanderson B M. 2016. The scenario model intercomparison project (ScenarioMIP) for CMIP6. Geosci Model Dev, 9: 3461–3482

Riahi K, van Vuuren D P, Kriegler E, Edmonds J, O'Neill B C, Fujimori S, Bauer N, Calvin K, Dellink R, Fricko O, Lutz W, Popp A, Cuaresma J C, Kc S, Leimbach M, Jiang L, Kram T, Rao S, Emmerling J, Ebi K, Hasegawa T, Havlik P, Humpenöder F, Da Silva L A, Smith S, Stehfest E, Bosetti V, Eom J, Gernaat D, Masui T, Rogelj J, Strefler J, Drouet L,

Krey V, Luderer G, Harmsen M, Takahashi K, Baumstark L, Doelman J C, Kainuma M, Klimont Z, Marangoni G, Lotze-Campen H, Obersteiner M, Tabeau A, Tavoni M. 2017. The shared socioeconomic pathways and their energy, land use, and greenhouse gas emissions implications: An overview. Glob Environ Change, 42: 153–168
Sheffield J, Goteti G, Wood E F. 2006. Development of a 50-year high-resolution global dataset of meteorological forcings for land surface modeling. J Clim, 19: 3088–3111
Skliris N, Zika J D, Nurser G, Josey S A, Marsh R. 2016. Global water cycle amplifying at less than the Clausius-Clapeyron rate. Sci Rep, 6: 38752
Su B D, Huang J L, Mondal S K, Zhai J Q, Wang Y J, Wen S S, Gao M N, Lv Y R, Jiang S, Jiang T, Li A W. 2021. Insight from CMIP6 SSP-RCP scenarios for future drought characteristics in China. Atmos Res, 250: 105375
Sun F, Mejia A, Zeng P, Che Y. 2019. Projecting meteorological, hydrological and agricultural droughts for the Yangtze River Basin. Sci Total Environ, 696: 134076
Sun J L, Lei X H, Tian Y, Liao W H, Wang Y H. 2013. Hydrological impacts of climate change in the upper reaches of the Yangtze River Basin. Quat Int, 304: 62–74
Tang Q H. 2020. Global change hydrology: Terrestrial water cycle and global change. Sci China Earth Sci, 63: 459–462
Teutschbein C, Seibert J. 2012. Bias correction of regional climate model simulations for hydrological climate-change impact studies: Review and evaluation of different methods. J Hydrol, 456-457: 12–29
van Vuuren D P, Edmonds J, Kainuma M, Riahi K, Thomson A, Hibbard K, Hurtt G C, Kram T, Krey V, Lamarque J F, Masui T, Meinshausen M, Nakicenovic N, Smith S J, Rose S K. 2011. The representative concentration pathways: An overview. Clim Change, 109: 5–31
Wang D, Liu M B, Chen X W, Gao L. 2021. Spatial and temporal variations of blue and green water resources in Shanmei reservoir watershed based on CMIP5 and SWAT (in Chinese). South-to-North Water Divers Water Conserv Sci Tech (Chin and Eng), 19: 446–458
Wang G Q, Zhang J Y, Jin J L, Pagano T C, Calow R, Bao Z X, Liu C S, Liu Y L, Yan X L. 2012. Assessing water resources in China using PRECIS projections and a VIC model. Hydrol Earth Syst Sci, 16: 231–240
Wang Y Q, Yang X L, Zhang M R, Zhang L Q, Yu X H, Ren L L, Liu Y, Jiang S H, Yuan F. 2019. Projected effects of climate change on future hydrological regimes in the upper Yangtze River Basin, China. Adv Meteorol, 2019: 1545746
Wang Z L, Zhong R D, Lai C G, Zeng Z Y, Lian Y Q, Bai X Y. 2018. Climate change enhances the severity and variability of drought in the Pearl River Basin in South China in the 21st century. Agric For Meteorol, 249: 149–162
Warszawski L, Frieler K, Huber V, Piontek F, Serdeczny O, Schewe J. 2014. The Inter-Sectoral Impact Model Intercomparison Project (ISI-MIP): Project framework. Proc Natl Acad Sci USA, 111: 3228–3232
Watterson I G. 2008. Calculation of probability density functions for temperature and precipitation change under global warming. J Geophys Res, 113: D12106
Wu Z Y, Chen X, Lu G H, Xiao H, He H, Zhang J H. 2017. Regional response of runoff in CMIP5 multi-model climate projections of Jiangsu Province, China. Stoch Environ Res Risk Assess, 31: 2627–2643
Wu Z Y, Lu G H, Wen L, Lin C A. 2011. Reconstructing and analyzing China's fifty-nine year (1951–2009) drought history using hydrological model simulation. Hydrol Earth Syst Sci, 15: 2881–2894
Xu L L, Wang A H. 2019. Application of the bias correction and spatial downscaling algorithm on the temperature extremes from CMIP5 multimodel ensembles in China. Earth Space Sci, 6: 2508–2524
Yamazaki D, Kanae S, Kim H, Oki T. 2011. A physically based description of floodplain inundation dynamics in a global river routing model. Water Resour Res, 47: W04501
Yang K, He J, Tang W J, Qin J, Cheng C C K. 2010. On downward shortwave and longwave radiations over high altitude regions: Observation and modeling in the Tibetan Plateau. Agric For Meteor, 150: 38–46
Yang Y, Pan M, Beck H E, Fisher C K, Beighley R E, Kao S C, Hong Y, Wood E F. 2019. In quest of calibration density and consistency in hydrologic modeling: Distributed parameter calibration against streamflow characteristics. Water Resour Res, 55: 7784–7803
Yang Y, Pan M, Lin P, Beck H E, Zeng Z, Yamazaki D, David C H, Lu H, Yang K, Hong Y, Wood E F. 2021. Global reach-level 3-hourly river flood reanalysis (1980–2019). Bull Am Meteorol Soc, 102: E2086–E2105
Yao Y, Qu W, Lu J X, Cheng H, Pang Z G, Lei T J, Tan Y A. 2021. Responses of hydrological processes under different shared socioeconomic pathway scenarios in the Huaihe River Basin, China. Water, 13: 1053
Xie Z. 2016. Dataset of estimation on channel section flow and stage in the midstream of the Heihe River Basin (1979–2014). National Tibetan Plateau Data Center
Zhang J M. 2020. Preliminary assessment of climate change in the Lancang River Basin based on CMIP6 data set (in Chinese). Master's Dissertation. Nanjing: Nanjing University of Information Science & Technology
Zhang X J, Tang Q, Pan M, Tang Y. 2014. A long-term land surface hydrologic fluxes and states dataset for China. J Hydrometeorol, 15: 2067–2084
Zhang Y, You Q L, Chen C C, Ge J. 2016. Impacts of climate change on streamflows under RCP scenarios: A case study in Xin River Basin, China. Atmos Res, 178-179: 521–534
Zhao Y, Li Z S, Cai S Y, Wang H. 2020. Characteristics of extreme precipitation and runoff in the Xijiang River Basin at global warming of 1.5°C and 2°C. Nat Hazards, 101: 669–688
Zhou Y S, Li X, Zheng D H, Li Z W, An B Y, Wang Y Z, Jiang D C, Su J B, Cao B. 2021. The joint driving effects of climate and weather changes caused the Chamoli glacier-rock avalanche in the high altitudes of the India Himalaya. Sci China Earth Sci, 64: 1909–1921
Zhu H H, Jiang Z H, Li J, Li W, Sun C X, Li L. 2020. Does CMIP6 inspire more confidence in simulating climate extremes over China? Adv Atmos Sci, 37: 1119–1132

(Responsible editor: Xin LI)